Materials Research Proceedings 28 (2023) 1511-1520 https://doi.org/10.21741/9781644902479-163

Modelling of yield point phenomenon in bake-hardening grade steel

DESHMANE Nachiket S.[1,2,a*], PERDAHCIOGLU Semih E. [1,b], and VAN DEN BOOGAARD Ton[1,c]

[1]University of Twente, Drienerlolaan 5, 7522 NB Enschede, Netherlands

[2]Stichting Materials innovation institute, Van der Burghweg 1, 2628 CS Delft, Netherlands

[a]nsdeshmane@gmail.com, [b]e.s.perdahcioglu@utwente.nl, [c]a.h.vandenboogaard@utwente.nl

Keywords: Yield Point Phenomenon, Lüders Bands, Strain Localization, Strain Gradient, Mesh Size Dependency

Abstract. In this study the yield point phenomenon in Bake-Hardening grade steel is predicted using a physically based thermo-mechanical model. A modified Taylor equation is proposed with a physically based dislocation density evolution approach. The softening that follows the higher yield point is incorporated with a Voce type decaying exponential function. The strain rate dependency of the plastic hardening is also incorporated in the model. The yield point in the decay function is also strain rate dependent but does not follow the same dependency of plastic hardening. This was solved by making the decay function strain rate dependent by adding a modified strain rate stress term to the exponential function. This parameter is calculated based on tensile experiments. Due to the softening behavior of the material, the numerical model is mesh size sensitive. Hence, a lower order strain gradient enhanced approach is implemented. The gradient is in a form of an additional hardening term assigned in the locally strained bands based on the plastic strain gradient. Hill48 yield criterion is used to assimilate the anisotropy in the steel grade. The numerical results show good correspondence with experimental tensile tests. The regularization significantly reduced the mesh size dependency of the numerical results.

Introduction

The yield point phenomenon creates an inhomogeneous plastic yielding in steels during forming, which results in unfavorable surface defects in form of stretcher marks on the formed steel products. Hence, modeling the yield point phenomenon has been a point of interest for many researchers in past few decades.

In a tensile test, the yield point phenomenon exhibits a distinct higher yield point followed by softening and a constant stress yield elongation, prior plastic hardening. Hahn [1] attributed the higher yield point to the extra stress required to unpin the locked dislocations by the Cottrell atmosphere. The unpinned dislocations are now mobile and multiply due to short range interaction with other dislocations resulting in a softening of the curve. A locally strained shear band(s) is(are) formed near the specimen shoulder at about 54° to the tensile axis and propagates along the tensile axis to the other shoulder of the specimen, termed as Lüders band. Hahn [1] was among the earlier researchers to propose an analytical model for the yield point phenomenon as an extended Orowan's equation based on dislocation density evolution and the dependency of the Lüders band velocity on the applied stress. Yoshida et al. [2] further proposed a constitutive model based on an extended Hahn model. They considered two modes the Lüders propagation and the subsequent plastic deformation with different sets of constitutive equations, the transition between the two was governed by a change in strain rates. Similarly, Estrin et al. [3, 4] and McCormick et al. [5] proposed a constitutive model for yield phenomena incorporating the dislocation dynamics based on diffusion of the dislocations to active slip systems on surrounding grains and their short-range interaction with immobile dislocations and solutes.

Contrary to Hahn's theory, Akama et.al [6] and Nes et al. [7] observed that the phenomenon is triggered not only by the release of dislocations locked by the Cottrell atmosphere but also by substitutional elements segregated at the grain boundaries. Nes et al. [7], therefore proposed a Taylor based dislocation density evolution equation [8] to incorporate grain size and dislocation cell size dependency, along with a thermally dependent parameter. Similarly, Ballarin et al. [9] developed a physically based model for bake-hardening steels to predict the macroscopic behavior based on carbon solute concentration, wherein the band propagation was modeled with a Voce type equation. Kyriakides et al. [10] modelled the Lüders phenomenon with a trilinear stress-strain curve with an intermediate softening response in bending of steel tubes. Span and van Liempt [11], proposed a physically based dislocation density evolution model for temper rolling that quantitatively described the Lüders band behavior in conjugation to temper rolling parameters and chemical composition of a particular steel grade. The softening in the model was attributed to the Lüders front velocity.

As stated earlier, in a tensile test, the yield point phenomenon is accompanied by a peak stress followed by a softening, which results in an inhomogeneous localized plastic shear band. In a finite element framework, this shear band is associated with the localization of strain along row(s) of elements. Simultaneously, the adjoining elements along this localized strain band undergo softening to compensate for the instability. Therefore, the band width, the strain gradient across the band and the resultant macroscopic flow stress (within Lüders strain elongation region) are mesh dependent [2,9,10,12]. Therefore, a regularization solution serves two objectives: firstly, to attain mesh–independent finite element results and secondly to account for the correlation of numerical Lüders band width to the actual observed in experiments. The regularization can be achieved by either introducing rate dependency to the model [10] or by introducing a higher order strain gradient to the model [12,13]. Kyriakides et al. introduced a mild rate dependency in the model via a strain rate power law, for the regularization of the solution. Mazière et al. [12] introduced the Aifantis strain gradient plasticity model, wherein a higher order modulus and a characteristic length scale is introduced, the latter being fitted with experiments. In this study, the mesh size dependency is reduced by using a lower-order gradient enhanced approach by the addition of a hardening term based on studies by Perdahcioglu et al. [14].

In the current study, a novel approach is modelled expanding on Taylors equation to incorporate thermal and strain rate dependency of the yield phenomena. The softening, or decay, function expands on the similar concept of dislocation density evolution and its short range interaction with immobile or mobile dislocations and solutes. This gives a better prediction of the Lüders phenomena in the model. Tensile tests to characterize Lüders phenomenon are elaborated in *Section Tensile Experiment*. The strain distribution and evolution over the specimen surface are captured with digital image correlation (DIC). A constitutive model detailed in section *Model* is proposed based on underlying physical dislocation density evolution. An extended Taylor model [8] is proposed, wherein the evolution of dislocation density is given by an extended Bergstrom model [15,16] for plastic hardening. For the softening an exponential equation is proposed. The model further incorporates strain rate dependency of the material based on Krabiell and Dahl [17] model. Based on experiments an anisotropic yield criteria Hill48 is used. The Lüders band width and strain distribution is observed to be mesh size sensitive. Hence a regularization method as proposed by Perdahcioglu et al. [14] is adopted to reduce the mesh size dependency of the numerical results; detailed in the section *Gradient Plasticity*. Finally the experimental and model results are discussed in the *Results and Discussion* as well as in the section *Conclusion*.

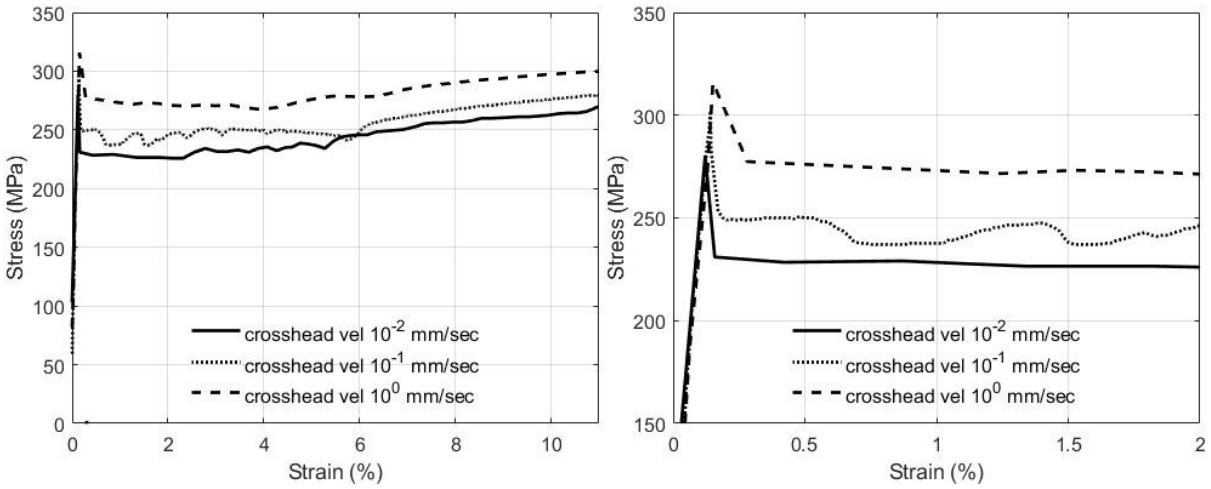

Fig. 1. Experimental tensile test of as-received Bake Hardened steel at three cross-head velocities.

Tensile Experiments

Bake hardening steel utilized in this study is in as-received state without undergoing temper rolling. Thus, the steel displays a distinctive yield point phenomenon with an elongated Lüders strain at a constant lower yield stress, see Fig. 1. The band is observed to nucleate just prior to higher yield point near the specimen shoulder and propagates across the specimen gauge length as the test progresses at a constant stress. The specimen is tested at three different cross-head velocities 10^0, 10^{-1}, 10^{-2} mm/s and at rolling, transverse and 45° direction. The local strain distribution and evolution across the specimen surface is measured with DIC during the tensile test. The surface of the specimen (gauge length) is therefore covered with a speckled pattern for the DIC (Aramis) measurement.

The higher yield point is observed to be linearly dependent to strain rate. Similarly, the Lüders stress and elongation are observed to be strain rate dependent. In each test, the band nu- cleated near the specimen shoulder at approximately 54° to the tensile loading axis and propagated along the loading axis across the gauge length. The band and its strain gradient could be seen in the DIC full field measurements Fig. 2 over the gauge length for the tensile test results at 10^{-1} cross head velocity. The band width is measured at half height with reference to the band (strain rate) peak height in this study. The mean peak width thus measured at half height was 5.6mm with a standard deviation of 0.79. The Lüders strain elongation is also observed to be directly proportional to the test cross-head velocity, and is in accordance with studies by Yoshida et al. It is also peculiar to see that the band does not limit to a single shear band, but forms a combination of two bands in a 'V' shape. A few tests also showed multiple bands being nucleated at both specimen shoulders during the test. It can be speculated that the band nucleation and propagation in a tensile test is a product of two factors: the dislocation density mechanics and the geometry of the test specimen. During band nucleation, the local shearing strain in a grain expands to neighboring grains, which deform in a preferred orientation resulting in a macroscopic shear band. Furthermore, the limitation imposed by the specimen width, causes the band to propagate during tensile loading.

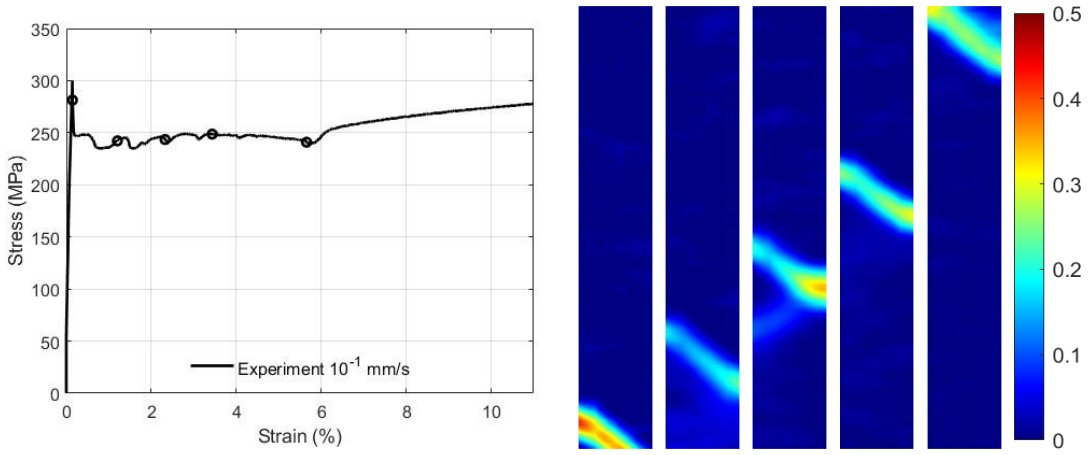

Fig. 2. Strain rate across the gauge length is plotted by DIC field measurements at stages highlighted in the flow stress.

Model

Work hardening.

A physically-based model, based on extended Taylor's equation is proposed in this study. The model therefore includes the dependency of flow stress in material on strain rate and temperature, and dislocation density evolution as a product of strain hardening.

$$\sigma(\epsilon) = \sigma_0 + \sigma_{thermal} + \sigma_{decay} + \alpha G b\sqrt{\rho(\epsilon)} \quad (1)$$

Where, σ_0 is the initial flow stress (MPa), $\sigma_{thermal}$ is the dynamic stress based on Krabiell and Dahl model [17], σ_{decay} is the softening function, α is constant parameter depending on immobile dislocations distribution, G is the shear modulus for steel, b is the Burgers vector, $\rho(\epsilon)$ is the dislocation density. Van Liempt [18] proposed an extended Bergstrom model [15] to show the dislocation density ρ development with strain. Eq. 2 describes the hardening as a development of the dislocation structure with strain.

$$\frac{d\rho}{d\epsilon} = M[B\rho^c\, g(\epsilon_t)] - \Omega\rho. \quad (2)$$

Where, ϵ gives total accumulated strain, B_u is the proportional constant for the increase of immobile dislocation in the cell walls, c is the exponent describing the influence of the dislocation density on the decrease of dislocation cell size, given by $d_{cell} = k\rho^{-c}$, M is the Taylor constant, parameter Ω is the strain rate and temperature dependent and represents the remobilization (dynamic recovery) of immobile dislocations. Here Ω is taken constant, β term provides for the linear hardening behavior at higher strains. The function $g(\epsilon)$ was introduced by van Liempt [18] to describe the change in dislocation mean free path due to change in dislocation cell geometry at higher strains. Vegter et al. [16,19] postulated that at high strains dislocation cell walls within the grains are deformed, and the small orientation difference between the cells influences the dislocation mean free path. This influence of the cell shape distortion on the mean free path is given with an exponential function $g(\epsilon) = \exp(\beta\epsilon)$. The first order term of Taylor series expansion of the function was used to avoid unexpected deflection at high strains in the flow stress giving the function: $g(\epsilon) = 1 + \beta\epsilon$. This gives a linear hardening at high strains, and by substituting the same in Eq. 2 the following is obtained:

$$\frac{d\rho}{d\epsilon} = M[B\rho^c\,(1 + \beta\epsilon_t)] - \Omega\rho. \quad (3)$$

Eq. 3 is integrated between the limits $\epsilon = 0$ and $\epsilon + \epsilon_0$, where ϵ_0 is the pre-deformation parameter accounting for the existing dislocation density prior to deformation, finally giving the dislocation density evolution as a function of equivalent strain as presented in Vegter et al. [19]:

$$\rho(\epsilon)^{\frac{1}{1-c}} = \frac{B_u}{\Omega}\left[\beta(\epsilon+\epsilon_0) + \left(1 - \frac{\beta}{M\Omega(1-c)}\right)\left[1 - \exp\left(-M\Omega(1-c)(\epsilon+\epsilon_0)\right)\right]\right] \quad (4)$$

This physically based density evolution is then substituted in Eq. 1 making the expression of the flow stress as a function of equivalent strain. The constants for the equation shown in Table 1 are referenced from [19].

Table 1. Parameters used for the hardening model.

σ_0	[MPa]	80
M	[-]	2.7
A	[-]	0.88
G	[MPa]	80.0E3
B	[-]	2.5E-7
Ω	[-]	2.1
B_u	[-]	8.3E8
B	[-]	0.38
ϵ_0	[-]	0.005
C	[-]	0.0

Dynamic stress.

The dynamic stress as postulated by Krabiell and Dahl [17], was incorporated into the model to account for the strain rate dependency of the material. The dynamic term describes the thermal activation of mobile dislocation past obstacles with regard to its dependency on strain rate and temperature.

$$\sigma_{thermal}(\dot{\epsilon}, T) = \begin{cases} 0 & \dot{\epsilon} < \dot{\epsilon}\exp\left(-\frac{\Delta G_0}{k_{boltz}T}\right) \\ \sigma_0^*\left(1 + \frac{k_{boltz}T}{\Delta G_0}\ln\frac{\dot{\epsilon}}{\dot{\epsilon_0}}\right)^p & \dot{\epsilon}\exp\left(-\frac{\Delta G_0}{k_{boltz}T}\right) < \dot{\epsilon} < \dot{\epsilon_0} \\ \sigma_0^* & \dot{\epsilon} > \dot{\epsilon_0} \end{cases} \quad (5)$$

Where, σ_0^* is the dynamic stress at zero thermal activation, ΔG_0 is the maximum activation enthalpy, p is the exponent for thermally activated contribution, $\dot{\epsilon_0}$ is a structure parameter pertaining to density of mobile dislocation and obstacle distribution; effectively the limiting strain rate for thermally activated movement, k_{boltz} is the Boltzmann constant and T is the temperature.

Decay stress.

The higher yield point can be attributed to either the additional stress required to unpin the locked dislocations in Cottrell atmosphere [1], or due to interaction of dislocation with grain boundaries [7] and the solutes segregated at grain boundaries [6]. Once the dislocations are 'free' from the obstacles, they become mobile. This can be considered as an instant drop in the number of immobile dislocations which causes a drop in the flow stress. An exponential Voce type equation is therefore proposed to represent the decay in the flow stress. It was also observed that the higher yield point is strain rate dependent and does not follow the work hardening strain rate

dependency. Thus, a modified Krabiell and Dahl [17] strain rate dependency model was implemented in σ_{decay} resulting in following equation:

$$\sigma_{decay} = \left(\Delta\sigma + \sigma_t^d\right) \exp(-n\epsilon) \tag{6}$$

Table 2. Thermal stress and Decay stress model parameters.

σ_0^*	[MPa]	1083
k_{boltz}	[mJ/K]	1.38E-20
T	[K]	300
ΔG_0	[mJ]	1.6E-16
$\dot{\epsilon}_0$	[-]	10.0E8
m	[-]	3.982
A	[-]	40
n	[-]	300

Where $\Delta\sigma$ corresponds to stress difference between higher yield point and yield point without the yielding phenomenon; the later estimated from Interstitial Free (IF) grade steel tests. This will correspond to the higher stress required to unpin the dislocations and set them to mobile phase. The exponential decay corresponds to the softening as a result of mobile dislocations multiplying by interaction with other dislocation networks and solutes. The constant n influences the softening rate due to dislocation multiplication. σ^d gives an additional stress term to the yield point, enabling strain rate dependency of the yield point. The parameters shown in Table 2 are fitted to experimental data by adjusting σ^* (from Eq. 5) keeping rest parameters constant.

Yield criterion.

The material exhibited anisotropy, with a variation in yield stress when tested under uniaxial and shear loading. Hill48 yield function was therefore used:

$$\phi = F\left(\sigma_y - \sigma_x\right)^2 + G(\sigma_z - \sigma_x)^2 + H\left(\sigma_x - \sigma_y\right)^2 + 2L\tau_{yz}^2 + 2M\tau_{zx}^2 + 2N\tau_{xy}^2 - \sigma_y^2 \tag{7}$$

The anisotropy coefficients, in terms of R values, were calculated from uniaxial and shear experiments. The model thereby showed a good fit with uniaxial tensile and shear test with same hardening parameters.

Gradient Plasticity.

The band size and strain gradient over the band showed mesh size dependency. Hence, the mesh size dependency is reduced using a lower-order gradient enhanced approach using an additional hardening term based on studies by Perdahcioglu et al. [14]. This non-local hardening term is calculated from the plastic strain gradients across the band. Perdahcioglu et al. [17] referred to this phenomenon as stress created by the evolution of geometrically necessary dislocations (GNDS) within a locally sheared zone and thus calculated them from incremental plastic strain and Burgers vector. The rate of change of the additional dislocations generated due to the strain gradient is therefore given by:

$$\dot{\rho}_{grad} = \frac{2\dot{\eta}^p}{b} \tag{8}$$

Where $\dot{\eta}^p$ is the rate of equivalent plastic strain gradient, b is the Burgers vector. The total change in dislocation density for a given strain increment ρ_{grad} is then placed in Eq. 1, resulting in an additional hardening stress across the band during its evolution and propagation.

$$\sigma(\epsilon) = \sigma_0 + \sigma_{thermal} + \sigma_{decay} + \alpha G b \sqrt{\rho(\epsilon) + \rho_{grad}} \quad (9)$$

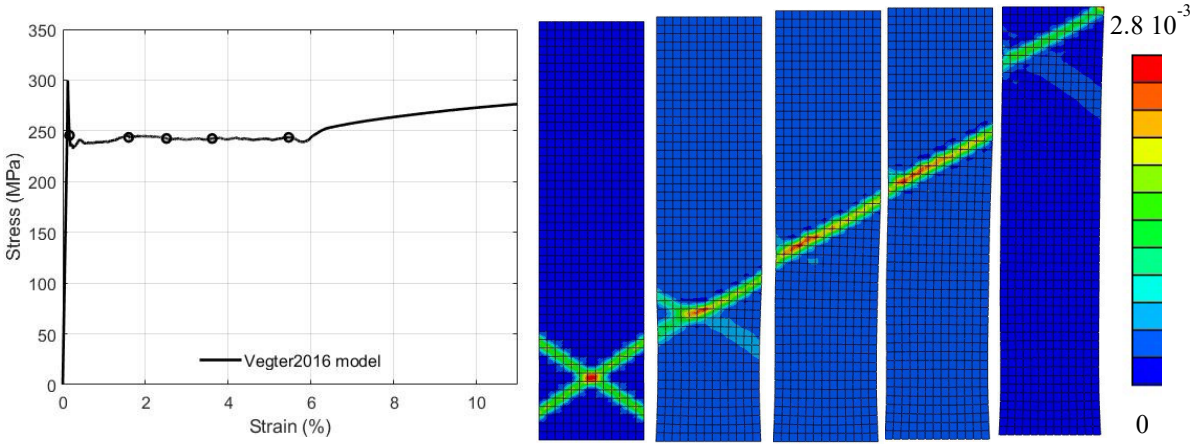

Fig. 3. Numerical tensile test strain-rate stages highlighted in flow stress.

Results and Discussions

The model was validated with a numerical tensile test. The gauge area 50x12.5x0.74 mm (length x width x thickness) was subjected to uniaxial loading. To replicate the material's inhomogeneity, numerical instability was incorporated by introducing fluctuating yield stress in a range 0 – 1 MPa randomly assigned to integration points. In Abaqus software, the arc-length method to solve for iterations during softening. The resultant flow stress and Lüders band are presented in Fig. 3. Fig. 4 shows the results of the simulations incorporating the hardening model combined with the anisotropic yield criterion tested at three cross-head velocities and shows a good fit with the experiments. The higher yield point is predicted well in the three velocities, attributed to the independent strain-rate model included in the decay function. The strain-rate dependency of the decay function also results in an increase in Lüders strain elongation with increasing test velocity. The thermal stress model's implementation shows a good fit with experimental tests at varying cross-head velocities. The band inclination is also observed between 52°-55° in accordance with the experiments.

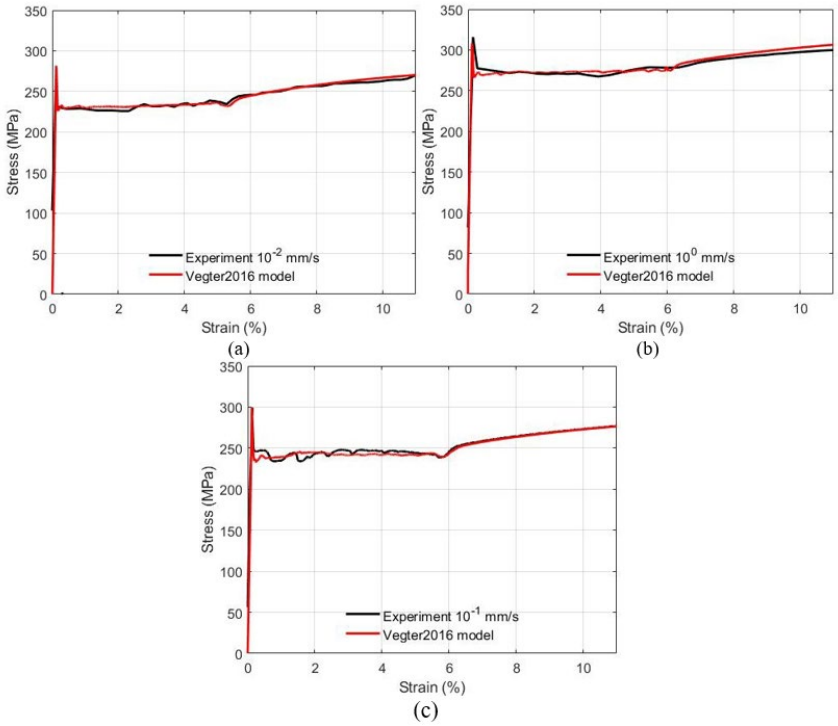

Fig. 4. Numerical tensile test compared with tensile experiments at three different cross-head velocities (a) 10^0 (b) 10^{-1} and (c) 10^{-2} mm/s.

Due to the softening and strain rate dependency in the model, the numerical test result is mesh dependent. Hence the first step was to test the mesh dependency of the model, by conducting the numerical tensile test by varying mesh sizes. Thus, numerical uniaxial tensile test was conducted with three-dimensional quadratic mesh with reduced integration at varying mesh sizes of 0.5, 0.75 and 1mm. The mean band peak width is calculated at every increment and plotted with reference to nodal displacement (Fig. 5 a). The mean peak width (calculated at half height of the peak) observed for mesh sizes 0.5, 0,75 and 1 mm are 1.30, 1.42 and 1.83mm. In either case the strain-rate peak is observed to be higher with a lower mesh size which further ascertains the mesh dependency of the Lüders band. The implementation of the gradient model results in an additional hardening term implemented only at the regions with localized strains, and is determined with a number of integration points within a prescribed radius. The integration points within the assigned radius experience an additional hardening term influencing the gradient width. This could be seen in the peak width determined from simulations with the gradient model, in Fig. 5b. Although a major difference could not be seen in the average peak widths for different mesh sizes, the variation of the peak width with different mesh sizes has more overlap with each other.

Summary

The modified dislocation density evolution model gives a good approximation of the experimental data. The dynamic stress factor implemented in the decay function enables predicting the higher yield point as well as Lüders elongation in coordination with applied strain rates. The decay function also facilitates understanding the underlying dislocation dynamics behavior: a higher yield stress term required to unpin the dislocations and an exponential decay to accommodate the softening by dislocation multiplication and short range interaction [1]. This includes its interaction with solutes at grain boundaries in accordance with [6]. It is also postulated that apart from dislocation dynamics, the specimen geometry in combination with its loading condition influences

formation of shear band and its propagation. The mesh size dependency of the strain bands was reduced by inclusion of the gradient model, however the simulated band size could not be achieved as observed in experiments. This could be further improved by modifying the decay function to control the rate of softening in the model.

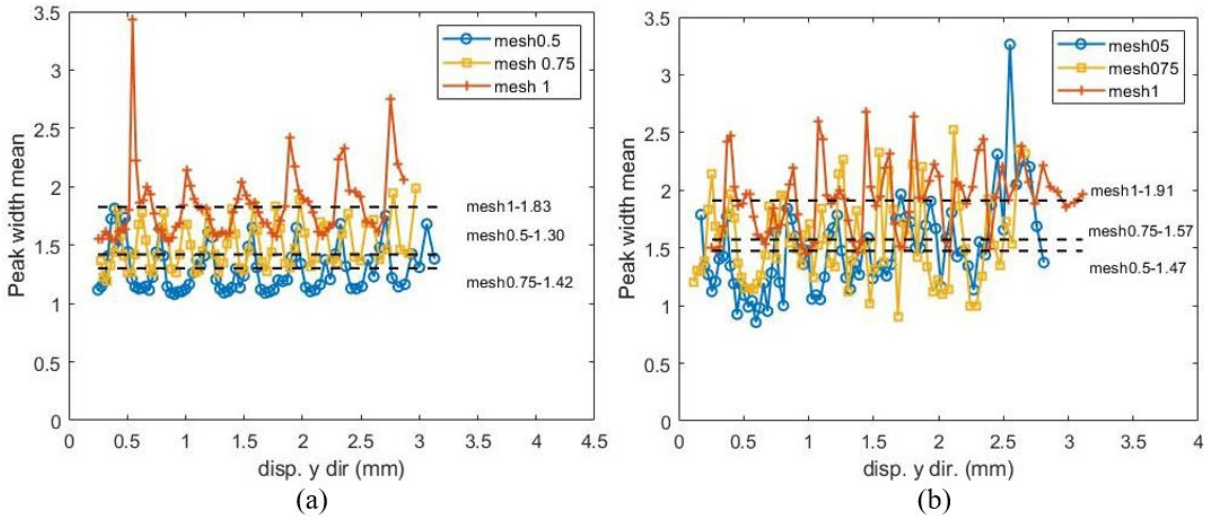

Fig. 5. For mesh sizes 0.5, 0.75 and 1mm band width with respect to displacement (a) without inclusion of gradient term (b) with inclusion of gradient term.

References

[1] G. Hahn, A model for yielding with special reference to the yield-point phenomena of iron and related bcc metals, Acta Metall. 10 (1962) 727–738. https://doi.org/10.1016/0001-6160(62)90041-X

[2] F. Yoshida, Y. Kaneda, S. Yamamoto, A plasticity model describing yield-point phenomena of steels and its application to fe simulation of temper rolling, Int. J. Plast. 24 (2008) 1792–1818. https://doi.org/10.1016/j.ijplas.2008.05.004

[3] Y. Estrin, L. Kubin, A unified phenomenological description of work hardening and creep based on one-parameter models, Acta Metall. 34 (1986) 2455–2464.

[4] Y. Estrin, L. Kubin, Plastic instabilities: phenomenology and theory, Mater. Sci. Eng. A 137 (1991) 125–134. https://doi.org/10.1016/0921-5093(91)90326-I

[5] P. McCormick, C. Ling, Numerical modelling of the portevin - le chatelier effect, Acta Metall. Mater. 43 (1995) 1969–1977. https://doi.org/10.1016/0956-7151(94)00390-4

[6] D. Akama, N. Nakada, T. Tsuchiyama, S. Takaki, A. Hironaka, Discontinuous yielding induced by the addition of nickel to interstitial-free steel, Scripta Mater. 82 (2014) 13–16. http://doi.org/10.1016/j.scriptamat.2014.03.012

[7] E. Nes, B. Holmedal, E. Evangelista, K. Marthinsen, Modelling grain boundary strengthening in ultra-fine grained aluminum alloys, Mater. Sci. Eng. A 410-411 (2005) 178–182. https://doi.org/10.1016/j.msea.2005.08.121

[8] G. Taylor, The mechanism of plastic deformation of crystals. part i. - theoretical, Royal Society 145 (1934).

[9] V. Ballarin, A. Perlade, X. Lemoine, O. Bouaziz, S. Forest, Mechanisms and modeling of bake-hardening steels: Part ii. complex loading paths, Metall. Mater. Trans. A 40 (2009) 1375–1382. http://doi.org/10.1007/s11661-009-9812-6

[10] S. Kyriakides, J. Miller, On the propagation of Luders bands in steel strips, J. Appl. Mech. 67 (2001) 645–654. https://doi.org/10.1115/1.1328348
[11] P. Span, J. van Liempt, Modelling of the impact of chemical composition on important metallurgical processes during cold strip production, EU technical Steel Res. (2005) 145–06.
[12] M. Mazière, S. Forest, Strain gradient plasticity modeling and finite element simulation of Lüders band formation and propagation, Cont. Mech. Thermodyn. 27 (2013) 83–104. https://doi.org/10.1007/s00161-013-0331-8
[13] M. Mazière, C. Luis, A. Marais, S. Forest, M. Gaspérini, Experimental and numerical analysis of the Luders phenomenon in simple shear, Int. J. Solid. Struct. 106 (2017) 305–314. https://doi.org/10.1016/j.ijsolstr.2016.07.026
[14] E. Perdahcıoglu, C. Soyarslan, T. Asık, E van den Boogaard, A class of rate-independent lower-order gradient plasticity theories: Implementation and application to disc torsion problem, Materials 11 (2018) 1425. https://doi.org/10.3390/ma11081425
[15] Y. Bergstrom, A dislocation model for the stress-strain behaviour of polycrystalline alpha-fe with special emphasis on the variation of the densities of mobile and immobile dislocations, Mater. Sci. Eng. 5 (1969) 193–200. https://doi.org/10.1016/0025-5416(70)90081-9
[16] H. Vegter, H. Mulder, P. van Liempt, J. Heijne, Tailored work hardening descriptions in simulation of sheet metal forming, Int. J. Plast. (2013) 474–481. https://doi.org/10.1063/1.4850016
[17] W. Krabiell, A. Dahl, Zum einfluß von temperatur und dehngeschwindigkeit auf die streckgrenze von baustählen unterschiedlicher festigkeit, Archiv fuer das Eisenhuettenwesen 52 (1982) 429–436.
[18] P. van Liempt, Workhardening and substructural geometry of metals, J. Mater. Process. Technol. 45 (1994) 459 – 464. https://doi.org/10.1016/0924-0136(94)90382-4
H. Vegter, H. Mulder, P. van Liempt, J. Heijne, Work hardening descriptions in simulation of sheet metal forming tailored to material type and processing, Int. J. Plast. 80 (2016) 204–221. https://doi.org/10.1016/j.ijplas.2015.11.002